

Search for Heavy Neutrinos in $\pi \rightarrow \mu\nu$ Decay

A. Aguilar-Arevalo^a, M. Aoki^b, M. Blecher^c, D.I. Britton^d, D. vom Bruch^{e,1}, D.A. Bryman^{e,f}, S. Chen^g, J. Comfort^h, L. Doria^{f,m}, S. Cuen-Rochin^e, P. Gumplinger^f, A. Hussein^{i,f}, Y. Igarashi^j, S. Ito^{b,n,*}, S.H. Kettell^k, L. Kurchaninov^f, L.S. Littenberg^k, C. Malbrunot^{e,o}, R.E. Mischke^f, T. Numao^{f,**}, D. Protopopescu^d, A. Sher^f, T. Sullivan^{e,p}, D. Vavilov^f

^aInstituto de Ciencias Nucleares, Universidad Nacional Autónoma de México, D.F. 04510 México

^bGraduate School of Science, Osaka University, Toyonaka, Osaka 560-0043, Japan

^cPhysics Department, Virginia Tech., Blacksburg, Virginia, 24061, USA

^dSchool of Physics and Astronomy, University of Glasgow, Glasgow, G12 8QQ, UK

^eDepartment of Physics and Astronomy, University of British Columbia, Vancouver, British Columbia, V6T 1Z1, Canada

^fTRIUMF, 4004 Wesbrook Mall, Vancouver, British Columbia, V6T 2A3, Canada

^gDepartment of Engineering Physics, Tsinghua University, Beijing, 100084, China

^hPhysics Department, Arizona State University, Tempe, Arizona, 85287, USA

ⁱUniversity of Northern British Columbia, Prince George, British Columbia, V2N 4Z9, Canada

^jKEK, 1-1 Oho, Tsukuba-shi, Ibaraki 305-0801, Japan

^kBrookhaven National Laboratory, Upton, New York, 11973-5000, USA

^lPresent address: LPNHE, Sorbonne Université, Paris Diderot Sorbonne Paris Cité, CNRS/IN2P3, Paris, France

^mpresent address: PRISMA Cluster of Excellence and Institut für Kernphysik Johannes Gutenberg-Universität Mainz, D 55128, Germany

ⁿPresent address: Faculty of Science, Okayama University, 3-1-1 Tsushimanaka, Kita-ku, Okayama, Japan 700-8530

^oPresent address: CERN, 1211 Geneva 21, Switzerland

^ppresent address: Department of Physics, Queen's University, Kingston, Ontario, K7L 3N6, Canada

Abstract

Heavy neutrinos were sought in pion decays $\pi^+ \rightarrow \mu^+ \nu$ by examining the observed muon energy spectrum for extra peaks in addition to the expected peak for a massless neutrino. No evidence for heavy neutrinos was observed. Upper limits were set on the neutrino mixing matrix $|U_{\mu i}|^2$ in the neutrino mass region of 15.7–33.8 MeV/c², improving on previous results by an order of magnitude.

Keywords: Pion decay, Heavy neutrino

1. Introduction

Neutrino oscillations indicate that at least two of the known neutrinos are massive, requiring the original Standard Model to be updated. The existence of additional heavy (mostly sterile) neutrinos is still an open question. A wide range of motivations [1] for heavy neutrinos come from considerations of baryogenesis [2], large scale structure formation [3], big bang nucleosynthesis [4], dynamical symmetry breaking [5], and other effects [6, 7]. In general, the mass scale of heavy neutrinos is unknown opening up many possibilities and potential observables in particle physics, astrophysics and cosmology. In the Neutrino Minimal Stan-

dard Model (ν MSSM) three sterile neutrinos are introduced which include a stable dark matter candidate [8]. MeV neutrinos could be accommodated in the ν MSSM to explain the ⁷Li abundance [9] or, with the addition of a MeV scalar, obtain consistent results for anomalies in neutrino experiments [10].

Massive neutrinos mixing with the muon neutrino in the mass region 1–400 MeV/c² have been sought by accelerator-based experiments studying pion [11, 12, 13, 14] and kaon decays [15, 16, 17]. The ratio of the $\pi^+ \rightarrow \mu^+ \nu_H$ decay rate to the normal $\pi^+ \rightarrow \mu^+ \nu$ decay rate can be written as

$$\frac{\Gamma(\pi^+ \rightarrow \mu^+ \nu_H)}{\Gamma(\pi^+ \rightarrow \mu^+ \nu)} = |U_{\mu i}|^2 \bar{\rho}(m_H) \quad (1)$$

for $|U_{\mu i}|^2 \ll 1$, where m_H is the mass of the heavy neutrino ν_H , $\bar{\rho}(m_H)$ accounts for the phase space and helicity suppression factors (normalized to the zero-mass

*Corresponding author: E-mail: s-ito@okayama-u.ac.jp

**Corresponding author: E-mail: toshio@triumf.ca

neutrino case) [18], and $U_{\mu i}$ is the neutrino mixing parameter for the weak muon-neutrino eigenstate ν_μ and the mass eigenstate ν_i .

Abela *et al.* [11] stopped pions in an active detector to measure the kinetic energy of muons from the decay $\pi^+ \rightarrow \mu^+ \nu$ (kinetic energy $T_\mu = 4.1$ MeV for a massless neutrino), and searched for low-energy peaks due to massive neutrinos. Upper limits on $|U_{\mu i}|^2$ for the 5–30 MeV/ c^2 region were set at a level of $10^{-2} - 10^{-5}$; the experiment was limited by accidental background. Massive neutrinos in the mass region 30–33.9 MeV/ c^2 were also sought in pion decay by Bryman and Numao [12], providing upper limits of $10^{-3} - 10^{-4}$; this search was limited by background coming from pion decays in flight (π DIF). Daum *et al.* [13] employed a similar technique but with excellent energy resolution using a Germanium detector; the search region was 1-20 MeV/ c^2 with a sensitivity level of 10^{-5} , which was limited by statistics. A dedicated magnetic spectrometer experiment [14] searched for a 33.9 MeV/ c^2 neutrino, providing a limit of a 10^{-8} level on $|U_{\mu i}|^2$. Figure 1 shows a summary of the present status of the search for massive neutrinos at 90% confidence level (CL) in the mass region 15.7–33.8 MeV/ c^2 .

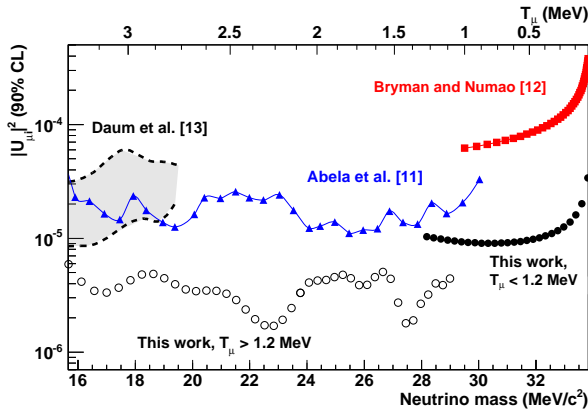


Figure 1: Summary of 90% CL upper limits on $|U_{\mu i}|^2$ vs m_H . The upper scale shows muon kinetic energy. The blue line and red dots indicate the previous limits by [11] and [12], respectively. Upper limits by [13] are located in the shaded region between the two dashed lines. The black closed-circles are the results of the present work for the region $0 < T_\mu < 1.2$ MeV and the black open circles for the region $1.1 < T_\mu < 3.3$ MeV.

The present search for massive neutrinos was based on measurement of the muon kinetic energy in $\pi^+ \rightarrow \mu^+ \nu$ decays at rest. When a pion is stopped in a thick plastic scintillator all decay vertices are contained; the first signal is from the kinetic energy of the incident beam pion, the second from the muon in $\pi^+ \rightarrow \mu^+ \nu$ decay, and the third from the positron in

$\mu^+ \rightarrow e^+ \nu \bar{\nu}$ decay ($\pi^+ \rightarrow \mu^+ \rightarrow e^+$ decay) which usually escapes in the case considered here. In the present study, the leading backgrounds arising from accidental particles and π DIF were suppressed using waveform and tracking information to identify extra activity in the detector system, and the statistics were improved by an order of magnitude over previous experiments.

2. Experiment

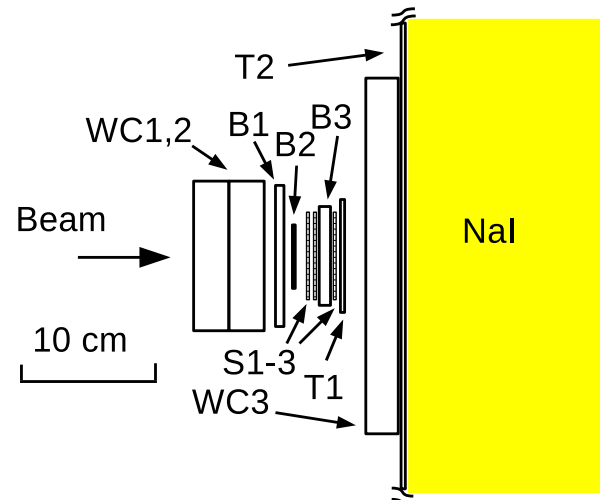


Figure 2: Cross-sectional view of the PIENU detector. CsI detectors surrounding the NaI crystal are not shown here.

The present search was carried out as a part of the PIENU experiment [19], a measurement of the branching ratio $\Gamma(\pi^+ \rightarrow e^+ \nu(\gamma))/\Gamma(\pi^+ \rightarrow \mu^+ \nu(\gamma))$ using pion decays at rest, where (γ) indicates inclusion of radiative processes.

Figure 2 shows a schematic view of the PIENU apparatus [20]. A 75-MeV/ c π^+ beam from the TRIUMF M13 channel [21] was degraded by two thin plastic scintillators B1 and B2 and stopped in an 8-mm thick plastic scintillator target (B3) at a rate of $5 \times 10^4 \pi^+$ /s. The pion stopping-depth distribution in B3 was centered with the RMS width of 0.7 mm. Pion tracking was provided by wire chambers (WC1 and WC2) at the exit of the beam line, and two X-Y sets of single-sided 0.3-mm thick planes of silicon strip detectors, S1 and S2, placed immediately upstream of B3. Positrons from $\mu^+ \rightarrow e^+ \nu \bar{\nu}$ decays were measured by another X-Y set of silicon strip detectors (S3), two thin plastic scintillators (T1 and T2), a set of wire chambers (WC3), and a calorimeter,

consisting of a 48-cm (dia.) \times 48-cm (length) single-crystal NaI(Tl) detector [22] surrounded by two concentric layers of pure CsI crystals [23].

A positron signal from muon decay (defined by a T1-T2 coincidence) in a time window between -300 and 540 ns with respect to the incoming pion was the basis of the main trigger with a rate of $3 \times 10^3 \text{ s}^{-1}$. This was prescaled by a factor of 16 to form an unbiased trigger (Prescaled trigger). Other triggers included a positron beam trigger for calibration and ones for enhancing rare $\pi^+ \rightarrow e^+ \nu$ decays. The typical trigger rate (including calibration triggers) was 600 s^{-1} . The number of Prescaled-trigger events used in this analysis was 4×10^9 .

3. Data processing and event selection

The charge and time of each scintillator pulse were extracted from the waveform recorded by a 500-MHz digitizer [24]. The charge for each pulse was obtained by integrating the pulse from -20 to 20 ns around the local maximum for plastic scintillators B1–3 and T1–2. Also, there were several integration windows for each detector system to accommodate specific purposes. Each readout channel was calibrated to the expected energy loss for 75-MeV/c beam particles. The nonlinear response of plastic scintillator was studied in a Monte Carlo simulation (MC) [25] and consistency was confirmed within 0.1 MeV.

Events originating from pions were selected based on their energy loss in B1 and B2, and the presence of a B3 hit. Events with extra activity other than that of the $\pi^+ \rightarrow \mu^+ \rightarrow e^+$ decay sequence in B1, B2, B3, T1 and T2 within the time region of -6.4 to $1.4 \mu\text{s}$ with respect to the pion stop were rejected. This significantly reduced the accidental background.

In order to ensure that an event was due to $\pi^+ \rightarrow \mu^+ \rightarrow e^+$ decay, the calorimeter energy was required to be <55 MeV and a loose geometrical positron acceptance cut (the radius of the hit position at WC3 to be <80 mm) was applied. The number of $\pi^+ \rightarrow \mu^+ \rightarrow e^+$ events was 5×10^8 .

A second pulse in B3 due to the muon kinetic energy needed to be identified in the search. However, when the muon energy involving ν_H was below 1.2 MeV the pulse detection logic could not efficiently identify the pulse. The search was, therefore, divided into two muon energy regions, above and below 1.2 MeV. In the region below 1.2 MeV the integrated energy up to 600 ns, containing the $\pi^+ \rightarrow \mu^+ \rightarrow e^+$ decay sequence, was examined for the muon energy contribution, while

in the region above 1.2 MeV the energy of a cleanly separated second pulse was used. In each analysis, all $\pi^+ \rightarrow \mu^+ \rightarrow e^+$ decay events were examined.

4. Analysis of the region below 1.2 MeV

Since the B3 energy observed with the wide time window included the pion and positron contributions in addition to the kinetic energy of the muon, these energies were first subtracted.

The contribution from the positron pulse, which resulted in a wider energy distribution due to the path length variation of the positron in B3, was subtracted using a well separated positron pulse in B3. In order not to affect the $\pi^+ \rightarrow \mu^+ \nu$ decay measurement, late positron time was required ($300 < t_{T1} - t_{B1} < 500$ ns).

In order to correct for the energy-loss variation of pions in the upstream detectors, the energies of the other beam counters (B1, B2, S1 and S2) were added for this search. Then, the contribution of the visible pion kinetic energy (~ 17 MeV) to the total energy was subtracted by shifting the spectrum to align the peak at 4.1 MeV. The black histogram in Fig. 3 shows the spectrum of the muon energy after the positron and pion energies were subtracted from the total energy.

The main background for this search is π DIF occurring very near or in B3, in which the observed ‘‘pion’’ energy can be less than the incident pion beam energy. The low-energy tail of the 4.1 MeV peak extending to $T_\mu = 0$ MeV was another background. The contribution from pion radiative decay $\pi \rightarrow \mu \nu \gamma$ was negligible.

The π DIF background was suppressed by two cuts [26]. The angle between the track vectors measured by WC1-2 (upstream) and S1-2 (near B3) provided a measure of a kink in the pion track due to π DIF. Limiting the kink angle suppressed the π DIF background as shown by the red histogram in Fig. 3. The muon decay vertex in the beam direction (Z-vertex) obtained from the pion (WC1-2 and S1-2) and positron (S3 and WC3) tracks also allowed identification of π DIF in B3 as shown by the green histogram. The low energy tail of the 4.1 MeV peak, mainly due to cleanly separated $\pi^+ \rightarrow \mu^+ \rightarrow e^+$ decays, was suppressed by a consistency test based on the difference of χ^2 values per degrees of freedom for two- and three-pulse fits. In this $\Delta\chi^2$ cut, only three pulse events with the second pulse falling into $T_{2nd} > 2$ MeV were rejected, so that the acceptance loss for the signal ($T_\mu < 1.2$ MeV) was negligible. After all cuts, the small but dominant background was still from π DIF in B3 as shown by the

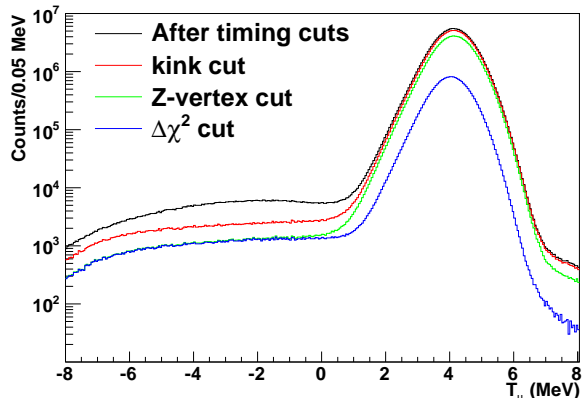


Figure 3: Energy spectra of muons for the $T_\mu < 1.2$ MeV analysis after subtraction of pion and positron energies from the total energy, with several cuts; black indicates the spectrum after the positron time cut, red after the angle cut, green after the Z vertex cut and blue after the $\Delta\chi^2$ cut.

blue histogram in Fig. 3.

4.1. Fit

There are two background shapes to be reproduced at energies above and below the signal region (0–1.2 MeV): the 4.1 MeV peak and the π DIF shape. The slightly asymmetric shape of the 4.1 MeV peak was mostly due to the kinetic energy distribution of the pions. The energy spectrum of events rejected by the $\Delta\chi^2$ cut was used to represent the background peak at 4.1 MeV. Since the events rejected by the $\Delta\chi^2$ cut had a bias due to the requirement of >2 MeV muon energy, the peak position and resolution were slightly different from those of the remaining events. The bias was compensated by multiplying the background peak by a unit Gaussian function with its center shifted by 0.1 MeV. The amplitude of the background peak and the resolution of the unit Gaussian were free parameters of the fit. A quadratic function was used for the π DIF background.

Figure 4 shows the fit using the two shapes described above. The fitting window of -4.0 to 3.5 MeV resulted in $\chi^2/ndof = 1.39$; there is some deviation above 2 MeV due to a small remaining mismatch in the resolution and peak position.

The signal peak in the region $T_\mu < 1.2$ MeV was assumed to be a Gaussian with a resolution offset. The resolution was scaled by the square root of the energy from that of the 4.1 MeV peak, and the offset was obtained from the pion-only peak (to represent a peak at 0 MeV) obtained from an 80-ns integration window with

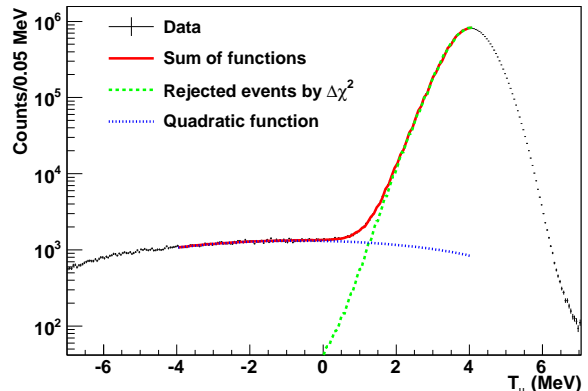


Figure 4: Fit results for the region $T_\mu < 1.2$ MeV. The black histogram, the blue dot and green dashed lines indicate data, quadratic background and the 4.1 peak, respectively. The smearing was applied in the plot.

a late muon pulse. The signal peak energy was varied from 0.0 MeV to 1.3 MeV with 0.05 MeV steps.

Figure 5 shows the signal amplitudes, with statistical errors, normalized to that of the 4.1 MeV peak (without the two-pulse requirement) after the acceptance correction of 1.06 for the Z-vertex cut; the distribution of the events in the 4.1 MeV peak was wider due to the longer muon range. Since no significant signal beyond the statistical fluctuation was observed, 90% CL upper limits on the neutrino mixing parameter $|U_{\mu i}|^2$ were obtained according to the Bayesian procedure assuming a positive peak amplitude with a Gaussian probability distribution. The full black circles for $0 < T_\mu < 1.2$ MeV (top axis) in Fig. 1 show the result.

5. Analysis of the region above 1.2 MeV

In this analysis the energy of the second pulse in the $\pi^+ \rightarrow \mu^+ \rightarrow e^+$ decay in B3 was used. The largest background was accidental background originating from decay of an “old” muon from an earlier pion or muon residing near B3 to a positron, giving a second or third pulse; some accidental background was already suppressed by the requirement of no additional coincident activity in the detectors. Radiative pion decay $\pi^+ \rightarrow \mu^+ \nu \gamma$ (branching fraction, 2×10^{-4} [27]) was about one tenth of the accidental background in the previous experiment [11].

Events with three separate pulses in B3 were selected in this analysis. Figure 6 shows energy spectra

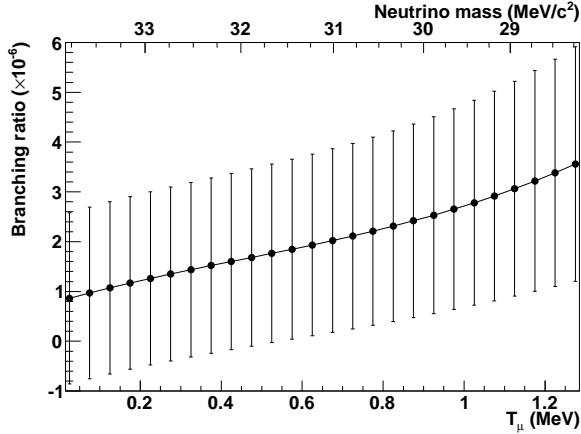


Figure 5: Normalized amplitudes (branching ratio) vs kinetic energy with statistical errors ($\pm 1\sigma$) after the Z-vertex acceptance correction. The upper scale shows m_H . Note: The step size is much smaller than the resolution.

of the second pulse with consecutive cuts described below. In order to clearly separate the positron pulse from the muon pulse, events with a late positron signal, firing T1 and the calorimeter in the positron time region $200 < t_{T1} - t_{B1} < 500$ ns, were selected. The second pulse was required to be within 80–150 ns with respect to the first pulse (pion stop). With this cut the energy variation due to the overshoot of the first pulse was minimized to < 0.16 MeV (a negligible level in terms of resolution).

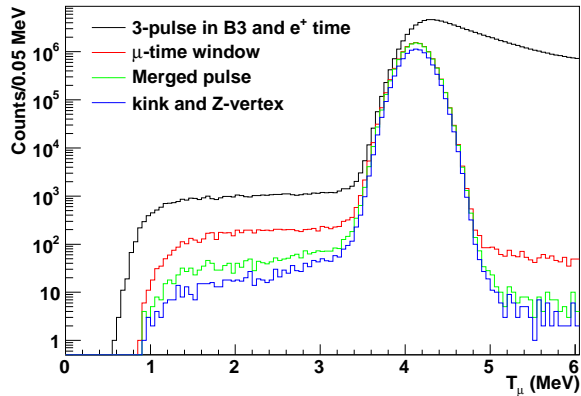


Figure 6: Energy spectra of the second pulse. The black line is for positrons in the 200–500 ns window as the third pulse, red with the time window cut of 80–150 ns for the second pulse, green with the merged-pulse cut in B3, and blue with the angle and vertex cuts.

The comparison of the pulse height and the integrated charge (–20 to 20 ns) of the first pulse identified early pion decays in which the muon pulse merges into the

first pulse and a positron pulse is recognized as the second. The effect is shown by the green histogram in Fig. 6. The kink angle and Z-vertex cuts reduced the contribution of π DIF. The total number of events used for the search in the region $T_\mu > 1.2$ MeV was 9×10^6 . After these cuts, the radiative pion decay $\pi^+ \rightarrow \mu^+ \nu \gamma$ was the major source of background.

5.1. Fit

The background shape for radiative pion decay was generated by MC [25] with the selection cuts, and the amplitude was a free parameter in the fit. A constant term (not in the final fit) was also added as a free parameter to represent other potential backgrounds, but it was always consistent with zero. The peak at 4.1 MeV was fitted with a Gaussian with the resolution, amplitude and position as free parameters. The acceptance losses due to the selection requirements were common to those of the peak at 4.1 MeV except for the pulse-detection logic which depended on the amplitude of the pulse (note the sharp drop around 1 MeV). This acceptance was estimated by comparing the observed positron energy spectrum with the MC positron spectrum which was not affected by the effects of the detection logic. Since the background events were also affected by the pulse detection logic, the fitting functions of the background and the signal were multiplied by this acceptance function.

A fit in the energy region $1.1 < T_\mu < 4.2$ MeV with a no-signal assumption provided a total $\chi^2 = 68$ with 58 degrees of freedom. The largest deviations were in the region above 3.4 MeV. Figure 7 shows the data in black and the result of the background fit in the red solid line. The small peak at 2 MeV (the red dashed line) indicates a hypothetical signal for $|U_{\mu i}|^2 = 1.5 \times 10^{-5}$.

For the search for additional peaks, the signal function, a Gaussian with the resolution scaled by the square root of the energy from that of the 4.1 MeV peak, was added to the fitting function. The signal peak was shifted in 0.05 MeV steps for the search. The amplitude of the signal peak was an additional free parameter of the fit. No significant excess above statistical fluctuations was observed. The amplitudes of hypothetical peaks normalized to the 4.1 MeV peak, with the Z-vertex acceptance correction, are shown in Fig. 8. The amplitudes in the region $T_\mu > 3.4$ MeV monotonically rise, reflecting a small deviation from the peak function. Since we did not see a significant excess in the signal amplitudes, a 90% CL upper limit on the mixing matrix $|U_{\mu i}|^2$ was set for each neutrino mass. The black open circles for $1.1 < T_\mu < 3.3$ MeV

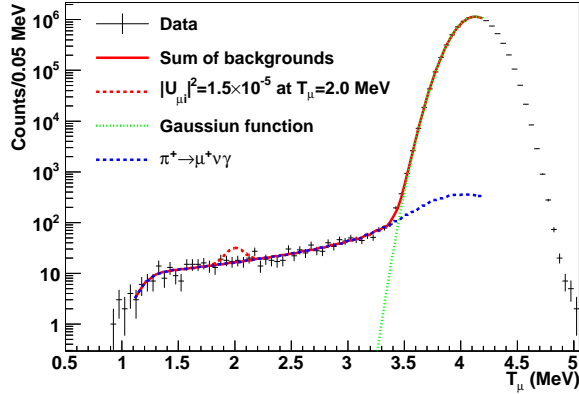


Figure 7: Data are shown by the black cross with statistical errors. The red lines are for the fit results without (solid) and with (dashed) a signal at 2 MeV for $|U_{\mu 1}|^2 = 1.5 \times 10^{-5}$. The green dotted line is for the 4.1 MeV Gaussian peak and the blue dashed line for the radiative decay background.

in Fig. 1 show 90% CL upper limits for $|U_{\mu i}|^2$.

6. Conclusion

No evidence for massive neutrinos in $\pi^+ \rightarrow \mu^+ \nu$ decay was observed. Upper limits on the neutrino mixing parameter $|U_{\mu i}|^2$ were obtained for the region $0 < T_\mu < 3.3$ MeV, which corresponds to $15.7 < m_H < 33.8$ MeV/ c^2 . The improvement factors were approximately an order of magnitude compared to the previous searches [11, 12, 13].

7. Acknowledgments

This work was supported by the Natural Sciences and Engineering Research Council and TRIUMF through a contribution from the National Research Council of Canada, and by the Research Fund for the Doctoral Program of Higher Education of China, by CONACYT doctoral fellowship from Mexico, and by JSPS KAKENHI Grant numbers 18540274, 21340059, 24224006, 19K03888 in Japan. We are grateful to Brookhaven National Laboratory for the loan of the crystals, and to the TRIUMF operations, detector, electronics and DAQ groups for their engineering and technical support.

References

- [1] M. Drewes, *Int. J. Mod. Phys. E* **22**, 1330019 (2013).

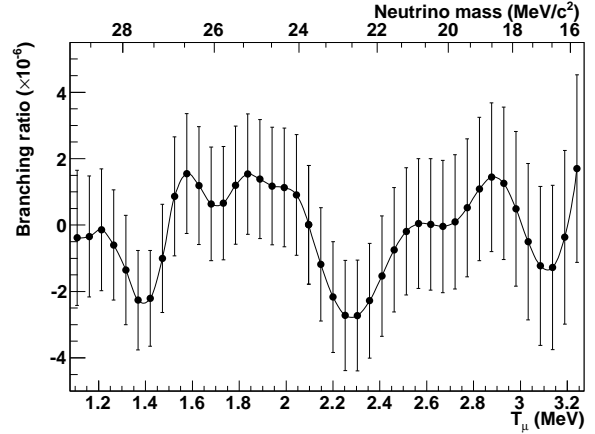


Figure 8: Normalized amplitudes (branching ratio) of the second pulse vs kinetic energy with statistical errors ($\pm 1\sigma$). The upper scale shows m_H .

- [2] L. Canetti, M. Drewes, and M. Shaposhnikov, *New J. Phys.* **14**, 095012 (2012).
[3] M. Viel *et al.*, *Phys. Rev.* **D71**, 063534 (2005).
[4] O. Ruchayskiy and A. Ivashko, *JCAP* **1210**, 014 (2012).
[5] T. Appelquist and R. Shrock, *Phys. Lett.* **B548**, 204-214 (2002).
[6] G. Gelmini *et al.*, *JCAP* **0810**, 029 (2008).
[7] B. Batell *et al.*, *Phys. Rev.* **D97**, 075016 (2018).
[8] T. Asaka, S. Blanchet and M. Shaposhnikov, *Phys. Lett.* **B631**, 151-156 (2005).
[9] H. Ishida, M. Kusabe and H. Okada, *Phys. Rev.* **D90**, 083519 (2014).
[10] J. Huang and A.E. Nelson, *Phys. Rev.* **D88**, 033016 (2013).
[11] R. Abela *et al.*, *Phys. Lett.* **105B**, 263 (1981).
[12] D.A. Bryman and T. Numao, *Phys. Rev.* **D53**, 558 (1996).
[13] M. Daum *et al.*, *Phys. Rev.* **D36**, 2624 (1987).
[14] M. Daum *et al.*, *Phys. Rev. Lett.* **85**, 1815-1818 (2000).
[15] R.S. Hayano *et al.*, *Phys. Rev. Lett.* **49**, 1305 (1982).
[16] A.V. Artamonov *et al.*, *Phys. Rev.* **D91**, 052001 (2015) and *Phys. Rev.* **D91**, 059903 (2015).
[17] E. Cortina Gil *et al.* (NA62 Collaboration), *Phys. Lett.* **B778**, 137 (2018).
[18] R.E. Shrock, *Phys. Rev.* **D24**, 1232 (1981).
[19] A. Aguilar-Arevalo *et al.*, *Phys. Rev. Lett.* **115**, 071801 (2015).
[20] A. Aguilar-Arevalo *et al.*, *Nucl. Instrum. Methods* **A791**, 38-46 (2015).
[21] A. Aguilar-Arevalo *et al.*, *Nucl. Instrum. Methods* **A609**, 102-105 (2009).
[22] Components borrowed from this experiment, G. Blanpied *et al.*, *Phys. Rev. Lett.* **76**, 1023 (1996).
[23] I-H. Chiang *et al.*, *IEEE Transactions on Nuclear Science* **NS-42**, 394 (1995).
[24] Y. Igarashi *et al.*, *IEEE Transactions on Nuclear Science* **NS-52**, 2866 (2005).
[25] S. Agostinelli *et al.* (GEANT4 collaboration), *Nucl. Instrum. Methods* **A506**, 250 (2003);
[26] A. Aguilar-Arevalo *et al.*, *Phys. Rev.* **D97**, 072012 (2018).
[27] G. Bressi *et al.*, *Nucl. Phys.* **B513**, 555 (1998).